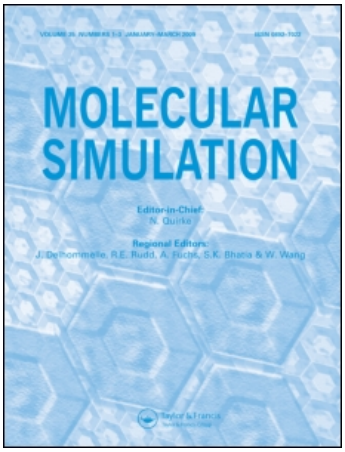


**Molecular Simulation**
Publication details, including instructions for authors and subscription information:
http://www.informaworld.com/smpp/title~content=t713644482

# Quantum chemistry of adsorption and hydrogenation of DBT and carbazole on NiMoS using ZINDO/I method

A. Duan[a]; J. Gao[a]; C. Xu[a]; D. Wang[a]; Z. Zhao[a]; T. Dou[b]; K. H. Chung[c]
[a] State Key Laboratory of Heavy Oil Processing, China University of Petroleum, Beijing, P. R. China [b] Key Laboratory of Catalysis, China University of Petroleum, Beijing, P. R. China [c] Syncrude Canada Ltd, Edmonton, Alta., Canada

**To cite this Article** Duan, A. , Gao, J. , Xu, C. , Wang, D. , Zhao, Z. , Dou, T. and Chung, K. H.(2007) 'Quantum chemistry of adsorption and hydrogenation of DBT and carbazole on NiMoS using ZINDO/I method', Molecular Simulation, 33: 4, 353 — 359
**To link to this Article: DOI:** 10.1080/08927020601133375
**URL:** http://dx.doi.org/10.1080/08927020601133375

*Molecular Simulation*, Vol. 33, Nos. 4–5, 15–30 April 2007, 353–359



# Quantum chemistry of adsorption and hydrogenation of DBT and carbazole on NiMoS using ZINDO/I method

A. DUAN†*, J. GAO†, C. XU†§, D. WANG†‖, Z. ZHAO†#, T. DOU‡** and K. H. CHUNG¶††

†State Key Laboratory of Heavy Oil Processing, China University of Petroleum, Beijing 102249, P. R. China
‡Key Laboratory of Catalysis, China University of Petroleum, Beijing 102249, P. R. China
¶Syncrude Canada Ltd, 9421-17 Avenue, Edmonton, Alta., Canada T6N 1H4

*(Received 15 June 2006; in final form 11 September 2006)*

The purpose of this study was to develop a fundamental understanding of the adsorption and first-step hydrogenation mechanisms of sulfur and nitrogen compounds over molybdenum disulfide ($MoS_2$). To do so, molecular simulation of the dibenzothiophene (DBT) and carbazole over NiMoS micro-crystal active surface was performed using Zerner's intermediate neglect of differential overlap (ZINDO) program with Hyperchem software. This study discusses the adsorbed structural parameters of DBT and carbazole molecules and proposes possible reaction pathways of hydrogenation on the NiMoS catalyst surface. The most stable configuration of adsorbed DBT is with the molecular plane perpendicular to the catalyst surface, while carbazole preferably adsorbed with the molecular plane parallel to the surface. Reaction enthalpies of DBT and carbazole adsorption processes on the catalyst surface were simulated based on the different configuration structures. The conformation heats and the activation energies of first-step hydrogenation of DBT and carbazole molecules over different configuration structures were also obtained by quantum chemistry simulation. The simulations on different catalyst surface structures indicated that the less vacant sites on the surface would result in the relatively low activation energies for DBT molecule. However, the hydrodenitrogenation (HDN) of carbazole increased with more vacant sites on the catalyst surface.

*Keywords*: Hydrodenitrogenation; Hydrodesulfurization; DBT; Carbazole; Quantum chemistry research; ZINDO-I



## 1. Introduction

Stringent environmental regulations for transportation fuels have accelerated the production of ultra clean fuels. Hydrotreating is one of the important industrial catalytic processes used to remove sulfur and nitrogen heteroatoms from petroleum distillates [1–3]. As a result of the demand for environmental friendly products, there is a renewed interest in the studies of hydrotreating catalyst design and reaction mechanisms.

Typical hydrotreating catalysts used in upgrading and refining are composed of nickel and molybdenum or tungsten (CoMo(W) or NiMo(W)) supported on $Al_2O_3$. They are usually prepared in an oxidic state and converted to a sulfidic state before use [4]. The CoMoS (or NiMoS) phase [5] is considered the active phase of cobalt (or nickel) promoted molybdenum sulfide catalysts, so more attention has been paid to its structure and reaction mechanism. A clear picture of the CoMoS (or NiMoS) phase has emerged from a combination of experimental and theoretical studies [6]. Quantum chemistry calculations have attracted more attention for theoretical study of reaction mechanisms and material design at the atomic level [7–11]. The structures of active phase on the different catalyst systems were proposed and the hydrotreating mechanisms of model compounds were also discussed [12–16].

*Corresponding author. Fax: +86-10-89731586. Email: duanaijun@cup.edu.cn
§Tel.: +86-10-89733392. Email: xcm@cup.edu.cn
‖Tel.: +86-10-89733733. Email: daxiw@163bj.com
#Tel.: +86-10-89731586. Email: zhenzhao@cup.edu.cn
**Tel.: +86-10-89733060. Email: doutao@cup.edu.cn
††Tel.: +1-780-9706885. Email: chung.keng@syncrude.com

*Molecular Simulation*
ISSN 0892-7022 print/ISSN 1029-0435 online © 2007 Taylor & Francis
http://www.tandf.co.uk/journals
DOI: 10.1080/08927020601133375

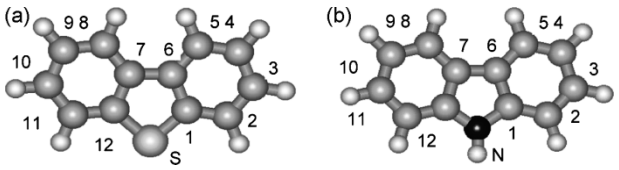


Figure 1. Molecule structures of DBT (a) and carbozole (b).

Ma *et al.* [12] proposed a single-slab cluster, $Mo_{27}S_{54}$, for modeling the highly dispersed $MoS_2$ based on the calculated edge structure, stoichiometric coordination of $MoS_2$ and the size of $MoS_2$ particles. Then the hydrodesulfurization (HDS) mechanism of thiophenic compounds over the proposed active phase model was simulated using Zerner's intermediate neglect of differential overlap (ZINDO) program. But the location of the active sites on $MoS_2$ surface for the hydrogenolysis of thiophenic compounds and hydrogenated thiophenic compounds, as well as the hydrogenolysis pathway was not addressed in this study. Morin *et al.* [13] addressed the different adsorption possibilities of thiophene ($C_4H_4S$) on the Ni(110) surface using the first principle local-density-functional calculations with the Vienna *ab initio* simulation package (VASP). The most stable adsorption structure of thiophene led to a thiol via an activated reaction with an energetic barrier of 0.70 eV. A description of the different transition states and a kinetic analysis of the desulfurization reaction were also presented. Nelson's group [14–16] systematically studied the energetics and surface structures of $MoS_2$, NiMoS, CoMoS, $WS_2$, NiWS and CoWS with *ab initio* density-functional theory (DFT) method. The dissociation of molecular hydrogen on the Ni-promoted $(10\bar{1}0)$ metal edge of NiMoS requires slightly lower activation energy than that on the unpromoted $(10\bar{1}0)$ Mo-edge of $MoS_2$. The addition of cobalt to the $(10\bar{1}0)$ S-edge significantly decreased the dissociation energy to approximately 0.6 eV. Based on this research, the adsorption and first-step hydrogenation of pyridine and pyrrole on the Ni-promoted $(10\bar{1}0)$ edge of $MoS_2$ were subsequently studied. The most stable configuration for adsorbed pyridine on the Ni-edge surface appeared to be with the molecular plane perpendicular to the surface through N—Ni bonding, while Pyrrole preferably interacted with the surface through the bonding of an α-carbon to a nickel site with the molecular plane flat on the surface.

Therefore, studies on the reaction mechanisms of HDS and hydrodenitrogenation (HDN) are essential to obtain further insight regarding the nature of active sites and intrinsic activation energies on the atomic level [4,6,10,16]. Presently, few studies related to the molecular simulations of DBT and carbazole have been found in open literature.

The ZINDO method is an effective molecular electronic program that has been developed in recent years [12,17,18]; the computing time to perform a ZINDO calculation is only a fraction of that required by first-principle programs. This study investigates the adsorption and first-step hydrogenation performance of dibenzothiophene (DBT) and carbazole on NiMoS using the ZINDO/1 method to elucidate HDS and HDN nano- and micromechanism pathways.

## 2. Method

The surface active phases in supported hydroprocessing catalysts are believed to follow the "Co–Mo–S" or "Ni–Mo–S" model [19,20]. In this model, the Mo(W) atoms are located in the center of a triangular prism surrounded by six S atoms and Co(Ni) atoms are located at the edge planes of the $MoS_2$ layered structure by replacement of the molybdenum atoms on either the $(\bar{1}010)$ or $(10\bar{1}0)$ edge planes. Sun *et al.* [16,18] verified this model and compared the energetics between different configurations. The incorporation of promoter atoms decreases the

Table 1. Quantum structural parameters of DBT and carbazole.

| | *DBT* | | | | *Carbazole* | | | | |
|---|---|---|---|---|---|---|---|---|---|
| *Angle* | *Bond/nm* | *Bond order* | *Atom* | *Charge/e* | *Angle* | *Bond/nm* | *Bond order* | *Atom* | *Charge/e* |
| C(1)C(2) | 0.1396 | 1.352 | C(1) | −0.271 | C(1)C(2) | 0.1400 | 1.357 | C(1) | 0.029 |
| C(2)C(3) | 0.1391 | 1.455 | C(2) | −0.101 | C(2)C(3) | 0.1394 | 1.429 | C(2) | −0.156 |
| C(3)C(4) | 0.1402 | 1.371 | C(3) | −0.118 | C(3)C(4) | 0.1400 | 1.397 | C(3) | −0.102 |
| C(4)C(5) | 0.1391 | 1.454 | C(4) | −0.134 | C(4)C(5) | 0.1395 | 1.425 | C(4) | −0.160 |
| C(5)C(6) | 0.1395 | 1.351 | C(5) | −0.090 | C(5)C(6) | 0.1387 | 1.381 | C(5) | −0.077 |
| C(6)C(1) | 0.1423 | 1.315 | C(6) | −0.052 | C(6)C(1) | 0.1447 | 1.273 | C(6) | −0.076 |
| C(7)C(12) | 0.1423 | 1.315 | C(7) | −0.052 | C(7)C(12) | 0.1447 | 1.273 | C(7) | −0.076 |
| C(6)C(7) | 0.1449 | 1.074 | C(8) | −0.090 | C(6)C(7) | 0.1453 | 1.079 | C(8) | −0.077 |
| C(7)C(8) | 0.1396 | 1.351 | C(9) | −0.134 | C(7)C(8) | 0.1388 | 1.381 | C(9) | −0.160 |
| C(8)C(9) | 0.1391 | 1.454 | C(10) | −0.118 | C(8)C(9) | 0.1395 | 1.425 | C(10) | −0.102 |
| C(9)S(10) | 0.1401 | 1.371 | C(11) | −0.101 | C(9)C(10) | 0.1400 | 1.397 | C(11) | −0.156 |
| C(10)C(11) | 0.1392 | 1.455 | C(12) | −0.271 | C(10)C(11) | 0.1394 | 1.429 | C(12) | 0.029 |
| C(11)C(12) | 0.1395 | 1.352 | S | 0.447 | C(11)C(12) | 0.1400 | 1.357 | N | −0.221 |
| C(12)S | 0.1700 | 1.067 | | | C(12)N | 0.1402 | 1.077 | | |

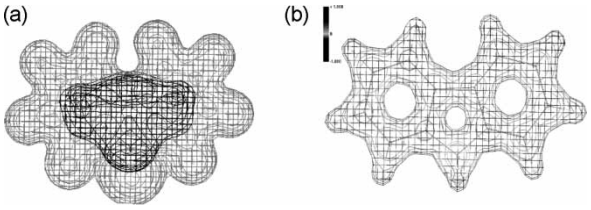


Figure 2. 3D isosurface (a) and 3D mapped isosurface (b) of electrostatic potential of DBT.

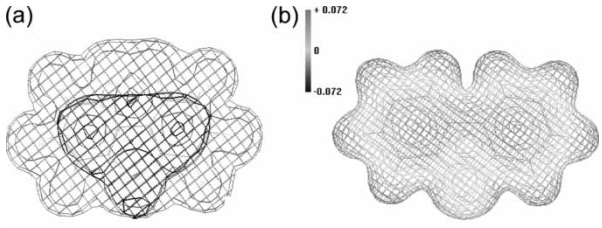


Figure 3. 3D isosurface (a) and 3D mapped isosurface (b) of electrostatic potential of carbazole.

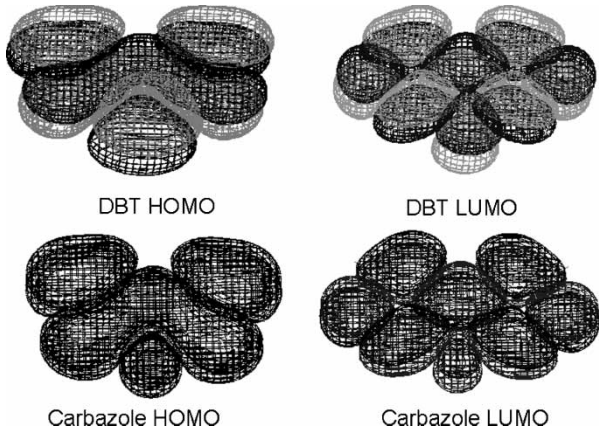


Figure 4. HOMO and LUMO orbits of DBT and carbazole.

binding energy of sulfur on the edge planes, reducing the equilibrium sulfur coverage on respective edge surfaces of promoted $MoS_2$ catalysts [14,21].

The structural parameters of the NiMoS micro-crystal unit have been reported by the previous paper [22]. The catalyst model in this study is constructed by the crystal builder module of Hyperchem 6.0.

Based on the configuration of the nano minicrystal catalyst structure, semi-empirical calculations were performed using the Hyperchem 6.0 ZINDO/1 method. The adsorptions and reactions of DBT and carbazole on active catalyst surfaces were simulated with the restricted-Hartree–Fock (RHF) and unrestricted-Hartree–Fock (UHF) methods, respectively.

## 3. Structural characterization of DBT and carbazole

DBT and carbazole with a double-ring structure usually were applied to study the mechanisms of HDS and HDN since they are one of the typical models of sulfur and nitrogen compounds [23,24]. Quantum chemistry calculations were carried out to obtain the relative structural parameters of DBT and carbazole by using the selection tool and display-label in Hyperchem. The structural schemes and the main properties are shown in figure 1 and table 1.

Based on the data in table 1, the bond lengths of the aromatic ring are slightly longer than the common C—C bond in benzene molecule. The asymmetrical bond lengths and bond order verified that the aromatic rings with $\pi$ bond were in activation states due to the conjugated effect of electron donor of heteroatoms—sulfur and nitrogen. The bond length of $C_{12}$—S is the longest and its bond order is the lowest in DBT molecule. However, in the carbazole molecule, the C—N bond is shorter than the C—S bond, and its bond order is also a little higher. This means that the C—N bond is more stable. Thus, nitrogen compounds are more difficult to remove than sulfur. The C—S bond is the easiest bond to split in the DBT molecule, so sulfur hydrogenolysis is the main route in HDS reaction.

Figures 2 and 3 are the 3D isosurface (a) and 3D mapped isosurface (b) of electrostatic potential of DBT and carbazole molecules. The 3D isosurface images in figures 2(a) and 3(a) indicate that the aromatic rings in these two molecules have electronegative properties. This implies that the aromatic rings have a relatively strong attraction to the cation sites. Thus the adsorption shapes of

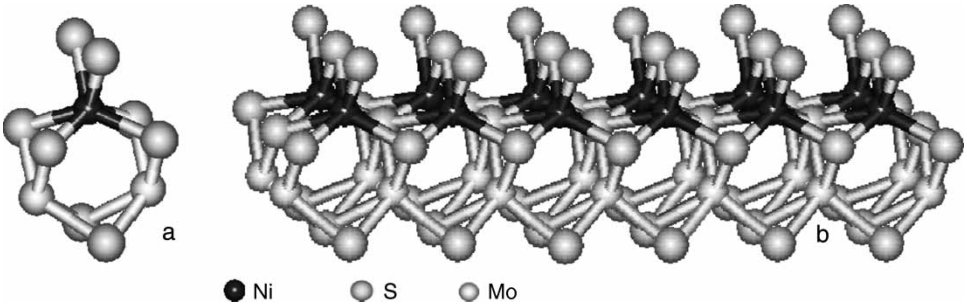


Figure 5. Sketch of catalyst crystal unit (a) and active phase surface (b).

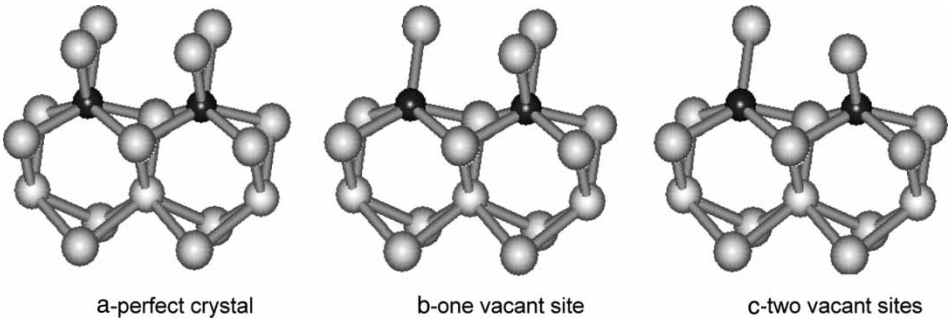


Figure 6. Sketches of catalyst with different vacant sites.

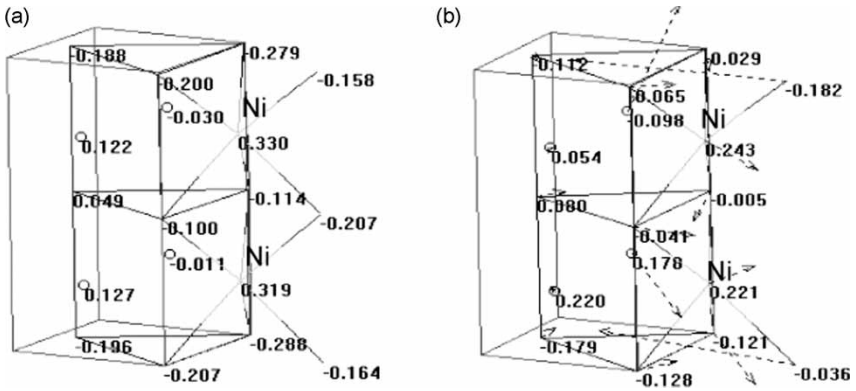


Figure 7. Comparison of charges on the surface of catalyst without vacancy (a) and with one vacant site (b).

these two molecules have two typical forms; perpendicular and parallel. Figures 2(b) and 3(b) also show that carbazole molecule has more potential for parallel adsorption on the catalyst surface than the DBT molecule. This is because the electronegative densities on aromatic rings and nitrogen atoms in the carbazole molecule have equivalent levels. The electronegative density on the sulfur atom exhibits a higher intensity than that on the aromatic ring in DBT molecule. This implies that DBT has more potential for perpendicular adsorption on the catalyst surface.

Figure 4 shows the 3D isosurface contours of the highest-occupied-molecular-orbit (HOMO) and lowest-occupied-molecular-orbit (LUMO) of DBT and carbazole. The orbital energies of DBT and carbazole were calculated by quantum chemistry simulation. The $HOMO_{DBT}$ was $-8.202$ eV, its $LUMO_{DBT}$ was $-0.40$ eV and the energy gap $\Delta E$ was 7.802 eV. For carbazole, $HOMO_{carb}$ was $-8.457$ eV, $LUMO_{carb}$ was $-0.156$ eV and $\Delta E$ was

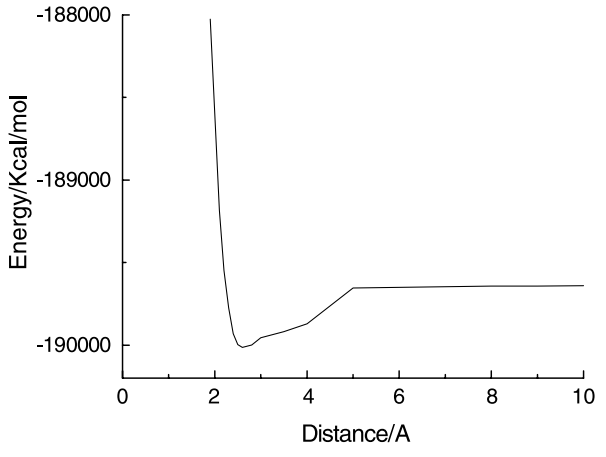


Figure 8. Energy trendline of DBT adsorbed on the catalyst with two vacant sites.

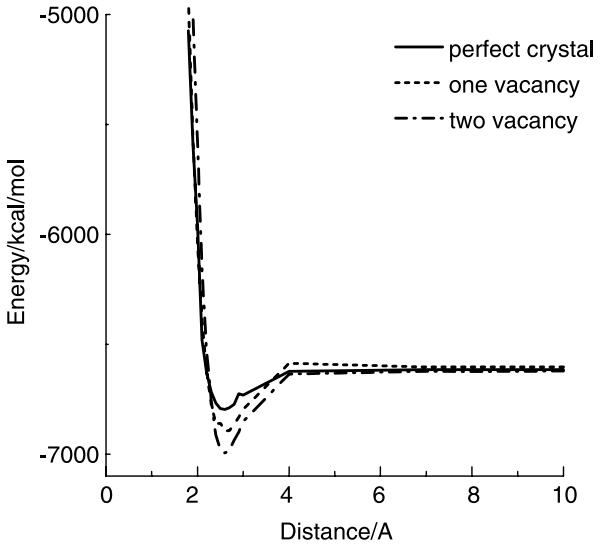


Figure 9. Energy trendline of carbazole adsorbed on different surface.

Table 2. Comparison of adsorption energies of DBT and carbazole.

| | *DBT* | *Carbazole* | | |
|---|---|---|---|---|
| *Energy/Kcal/mol* | *c* | *a* | *b* | *c* |
| Before adsorption | −7622.0 | −6616.2 | −6604.0 | −6612.6 |
| After adsorption | −7994.9 | −6796.9 | −6893.5 | −6984.6 |
| Energy difference | −372.9 | −180.7 | −289.5 | −372.0 |

Note: a, perfect crystal; b, one vacant site; and c, two vacant sites.

8.301 eV. Molecular orbital theory indicates that the low energy gap between HOMO and LUMO orbits favours high activity in reaction. Therefore, DBT will be more active than carbazole in the hydrogenation process.

## 4. Simulation of DBT and carbazole adsorptions on the catalyst surface

Based on the structure of the NiMoS phase [4,12,22], the configuration of the active phase on the catalyst surface are shown in figure 5. Different configurations of the active surface on the catalyst are shown in figure 6. Figure 7 shows the charges on the catalyst surface of perfect crystal and one sulfur vacant site. It can be seen that the charge in Ni atom on the one sulfur vacant site disfiguration is a little lower than that on perfect crystal, which facilitates the adsorption of anion and improves the hydrogenolysis of heteroatom compounds.

Simulation of the adsorption of DBT and carbazole molecules onto the catalyst surface was carried out to obtain the total energy changes of the adsorption process. Plots of Energy with adsorption distance are shown on figures 8 and 9. The corresponding adsorption heats over different surface configurations are listed in table 2.

The adsorption of DBT and carbazole molecules usually includes perpendicular and parallel modalities to the active surface. However, for large molecules, the stereochemical barrier from side-chains hinders the approach of reactant molecules to the active surface. This results in the parallel adsorption of reactant molecules to the active surface of the catalyst. For DBT and carbazole molecules, there are no side-chains around the heteroatom. Therefore, the most stable configuration for adsorbed DBT and carbazole molecules on the active site is with the molecular planes perpendicular to the catalyst surface through heteroatom–metal bonding.

Figures 8 and 9 and table 2 show that the adsorption process is exothermic, and the adsorption energies of DBT and carbazole on the configuration with two sulfur vacant sites were −372.9 and −372.0 kcal/mol, respectively. Since these values are almost the same, this indicates that these are the stable states of adsorbed DBT and carbazole molecules. The high values of the adsorption heats in table 2 also indicate that there are strong interactions existing between the reactant molecules and the catalyst surface. Furthermore, the total energy of system reached a minimum at a distance of 0.25 nm, which was very close to the length of a typical Ni—S (0.235 nm) chemical bond in the NiS molecule. As the reactant molecules approached to the active sites on catalyst surface, the internal electrostatic repulsion forces increased sharply, resulting in a rapid increase in the total system energy (figures 8 and 9).

The data in table 2 verifies that the more vacant sites on the catalyst that were available the lower the total energies were. Table 3 lists the quantum structural parameters of DBT and carbazole stably adsorbed on catalyst surface. Comparing the data in tables 1 and 3, the structural parameters before and after adsorption, it was found that some bond lengths increased, especially the C—S and C—N bond. Bond orders also decreased, indicating that the reactant molecules were kept on an active stable state after they were adsorbed on the catalyst surface. The C(12)—S was the weakest bond in DBT molecule, but in the carbazole molecule the C(11)C(12) was most likely to be attacked by H radicle in the hydrotreating process, so the hydrogenolysis route was the controlling step for DBT

Table 3. Quantum structural parameters of DBT and Carbazole adsorbed in catalyst.

| | *DBT* | | | | *Carbazole* | | | | |
|---|---|---|---|---|---|---|---|---|---|
| *Angle* | *Bond/nm* | *Bond order* | *Atom* | *Charge/e* | *Angle* | *Bond/nm* | *Bond order* | *Atom* | *Charge/e* |
| C(1)C(2) | 0.146 | 1.16 | C(1) | −0.21 | C(1)C(2) | 0.1479 | 0.0297 | C(1) | 0.102 |
| C(2)C(3) | 0.134 | 1.68 | C(2) | −0.096 | C(2)C(3) | 0.1468 | 0.0114 | C(2) | 0.112 |
| C(3)C(4) | 0.147 | 1.17 | C(3) | −0.12 | C(3)C(4) | 0.1454 | 0.0200 | C(3) | 0.108 |
| C(4)C(5) | 0.134 | 1.68 | C(4) | −0.133 | C(4)C(5) | 0.1352 | 0.316 | C(4) | −0.050 |
| C(5)C(6) | 0.146 | 1.16 | C(5) | −0.092 | C(5)C(6) | 0.1450 | 0.0348 | C(5) | −0.016 |
| C(6)C(1) | 0.134 | 1.53 | C(6) | −0.054 | C(6)C(1) | 0.1474 | 0.402 | C(6) | −0.009 |
| C(7)C(12) | 0.134 | 1.53 | C(7) | −0.054 | C(7)C(12) | 0.1445 | 0.0319 | C(7) | −0.017 |
| C(6)C(7) | 0.147 | 1.06 | C(8) | −0.092 | C(6)C(7) | 0.1471 | 0.654 | C(8) | 0.069 |
| C(7)C(8) | 0.146 | 1.16 | C(9) | −0.133 | C(7)C(8) | 0.1382 | 0.0205 | C(9) | −0.082 |
| C(8)C(9) | 0.134 | 1.68 | C(10) | −0.120 | C(8)C(9) | 0.1436 | $7.40 \times 10^{-4}$ | C(10) | 0.076 |
| C(9)S(10) | 0.147 | 1.17 | C(11) | −0.096 | C(9)C(10) | 0.1451 | $5.22 \times 10^{-4}$ | C(11) | 0.052 |
| C(10)C(11) | 0.134 | 1.68 | C(12) | −0.21 | C(10)C(11) | 0.1478 | $7.81 \times 10^{-3}$ | C(12) | 0.211 |
| C(11)C(12) | 0.146 | 1.16 | S | 0.319 | C(11)C(12) | 0.1480 | $8.21 \times 10^{-4}$ | N | −0.159 |
| C(12)S | 0.178 | 1.05 | | | C(12)N | 0.1425 | 0.0126 | | |

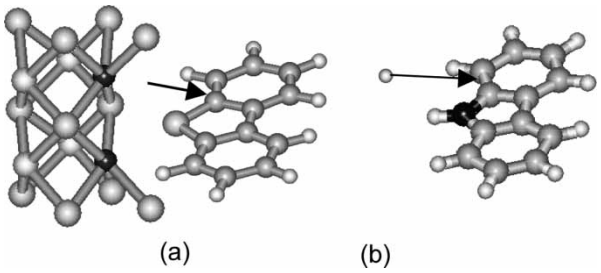


Figure 10. Scheme of hydrotreating process of DBT (a) and carbozole (b).

HDS, while the hydrotreating route dominated the HDN process for carbazole.

## 5. Simulation of hydrotreating reactions of DBT and carbazole molecules on catalyst surface

The reaction schemes for the hydrotreating process of DBT and carbazole molecules on the configuration with one sulfur vacant site are shown in figure 10. The first-step hydrogenation reactions of DBT and carbazole on active catalyst surfaces were simulated to obtain the energy trends with different configurations, as shown in table 4.

When the reactant molecules were strongly adsorbed onto the catalyst surface, the weakest bonds in the DBT and carbazole molecules reacted first. For DBT hydrotreating, the weakest bond is C—S cleavage and for carbazole is C(11)C(12) hydrogenation.

From the data in table 4, it was shown that the activation energies for DBT molecule hydrotreating over different surface structures were variable. The activation energies of the configurations with one or two vacant sites were relatively low, indicating that the suitable crystal configuration shape favors sulfur atom hydrogenolysis in the DBT molecule. For the carbazole molecule, the activation energies were much higher indicating that the reactivity of carbazole molecule was lower than DBT molecule. The more vacant sites existed on the catalyst configuration, the lower the activation energy was. As the number of sulfur vacant sites increases from 1 to 2, the activation energies of DBT hydrogenolysis didn't change significantly (22.17–25.34 kcal/mol). By comparison, for carbazole hydrotreating, the activation energy decreased from 143.30 to 61.13 kcal/mol. This is attributed to the different mechanisms of DBT and carbazole hydrotreating [21]. DBT can be reacted through the hydrogenolysis route directly, while carbazole needed to be hydrotreated first and then nitrogen atom to be removed. In the latter case, more active sites are needed to take part in these reactions.

The more coordinated vacant sites on the catalyst configuration, it was more easier for the reactant molecules to contacts the active sites. Consequentially, the reactions of hydrotreating and/or hydrogenolysis would proceed more smoothly under the same operating conditions. This provides some helpful information for catalyst oriented synthesis, catalyst design and preparation.

## 6. Conclusion

To develop a fundamental understanding of the adsorption and first-step hydrogenation mechanisms of sulfurous and nitrogenous compounds over molybdenum disulfide ($MoS_2$), molecular simulation of the DBT and carbazole over NiMoS micro-crystal active surface was performed using the ZINDO/1 program with Hyperchem software. This study discussed the adsorbed structural parameters of DBT and carbazole molecules and proposed the possible reaction pathways of hydrogenation on the NiMoS catalyst surface. The most stable configuration of adsorbed DBT is with the molecular plane perpendicular to the catalyst surface, whereas carbazole preferably adsorbed parallel to the surface. Reaction enthalpies of DBT and carbazole adsorption processes on the catalyst surface were simulated based on the different configuration structures. The conformation heats and the activation energies of first-step hydrogenation of DBT and carbazole molecules on the different configurations were obtained by quantum chemistry simulation. The simulation results indicated that the less vacant sites on the surface would result in the relatively low activation energies for DBT molecule, while carbazole HDN increased with more vacant sites on catalyst surface based on the structural effects on reaction barriers.

Table 4. Energy trend of DBT and carbazole hydrotreating over different configurations.

| *Energy/kcal/mol* | *DBT* | | | *Carbazole* | | |
|---|---|---|---|---|---|---|
| | *a* | *b* | *c* | *a* | *b* | *c* |
| $\Delta E$/kcal/mol | 43.74 | 22.17 | 25.34 | 155.50 | 143.30 | 61.13 |
| Before adsorption | −7235.6 | −7238.5 | −7360.3 | −7063.2 | −7036.4 | −7021.1 |
| After adsorption | −7273.8 | −7263.6 | −7392.3 | −7117.7 | −7123.2 | −7080.5 |
| Heat/kcal/mol | −38.18 | −25.06 | −32.04 | −54.46 | −86.32 | −59.42 |

Note: a, perfect crystal; b, one vacant site; and c, two vacant site.

## Acknowledgements

This research was supported by National Nature Science Foundation of China (no.20406012) and CNPC program (no.04A5050102 and 05E7019) and SKLHP open project 2004–06 of China University of Petroleum (Beijing).

## References

[1] Annual Refining Survey, *Oil Gas J.*, **53**, 49 (1996).
[2] J. Chang, J. Liu, D. Li. *Catal. Today*, **43**, 233 (1998).
[3] J. Chen. *Chin. Eng. Sci.*, **2**, 21 (2000).
[4] H. Topsøe, B.S. Clausen, F.E. Massoth. *Hydrotreating Catalysis, Science and Technology*, vol. 11, Springer, Berlin (1996).
[5] H. Topsøe, B.S. Clausen, R. Candia, C. Wivel, S. Morup. *In situ* Mössbauer emission spectroscopy studies of unsupported and supported sulfided Co—Mo hydrodesulfurization catalysts: Evidence for and nature of a Co—Mo—S phase. *J. Catal.*, **68**, 433 (1984).
[6] J.V. Lauritsen, S. Helveg, E. Lægsgaard, I. Stensgaard, B.S. Clausen, H. Topsøe, F. Besenbacher. Atomic-scale structure of Co—Mo—S nanoclusters in hydrotreating catalysts. *J. Catal.*, **197**, 1 (2001).
[7] P.R. Schleyer. *Encyclopedia of Computational Chemistry*, John Wiley & Sons, NewYork (1998).
[8] L. Tao. Orbital images to analyze the metallic catalytic reaction mechanism. *Chemistry*, **4**, 12 (1994).
[9] Y. Nakazaki, N. Goto, T. Inui. Simulation of dynamic behaviors of simple aromatic hydrocarbons inside the pores of a pentasil zeolite. *J. Catal.*, **136**, 141 (1991).
[10] P. Demontis, G.B. Suffritti. *Modelling of Structure and Reactivity in Zeolites*, C.R.A. Catlow (Ed.), Academic Press, London (1992).
[11] P. Raybaud, J. Hafner, G. Kresse. Structure, energetics, and electronic properties of the surface of a promoted $MoS_2$ catalyst: An *ab initio* local density functional study. *J. Catal.*, **190**, 128 (2000).
[12] X. Ma, H.H. Schobert. *J. Mol. Catal. A*, **160**, 409 (2000).
[13] C. Morin, A. Eichler, R. Hirschl, P. Sautet, J. Hafner. DFT study of adsorption and dissociation of thiophene molecules on Ni(1 1 0). *Surf. Sci.*, **540**, 474 (2003).
[14] M. Sun, A.E. Nelson, J. Adjaye. *J. Catal.*, **226**, 41 (2004).
[15] M. Sun, A.E. Nelson, J. Adjaye. *J. Catal.*, **233**, 411 (2005).
[16] M. Sun, J. Adjaye, A.E. Nelson. Theoretical investigations of the structures and properties of molybdenum-based sulfide catalysts. *Appl. Catal. A*, **263**, 131 (2004).
[17] Molecular Simulation, http://www.msi.com/science/online/references/ZINDO References.html, Jan (2000).
[18] W.P. Anderson, T.R. Cundarai, R.S. Drago, M.C. Zerner. Utility of the semiempirical INDO/1 method for the calculation of the geometries of second-row transition-metal species. *Inorg. Chem.*, **29**, 1 (1990).
[19] J. Grimblot. *Catal. Today*, **41**, 111 (1998).
[20] S.M.A.M. Bouwens, J.A.R. van Veen, D.C. Koningsberger. *J. Phys. Chem.*, **95**, 123 (1991).
[21] M. Sun, A.E. Nelson, J. Adjaye. *J. Catal.*, **231**, 223 (2005).
[22] Duan, C. Xu, J. Gao. *J. Mol. Struct.*, **734**, 89 (2005).
[23] T. Klimova, M. Calderón, J. Ramírez. *Appl. Catal. A*, **240**, 29 (2003).
[24] A. Szymánska, M. Lewandowski, C. Sayag, D. Mariadassou. Kinetic study of the hydrodenitrogenation of carbazole over bulk molybdenum carbide. *J. Catal.*, **218**, 24 (2003).